

## Transformations of photoluminescence spectra of upconversion nanophosphors by phantoms of biological tissues

© E.M. Trifanova<sup>1,¶</sup>, M.E. Nikolaeva<sup>2</sup>, A.P. Sviridov<sup>1</sup>, V.K. Popov<sup>1</sup>

<sup>1</sup> Institute of Photon Technologies (IPT), FSRC „Crystallography and Photonics“ of RAS, 108840 Moscow, Troitsk, Russia

<sup>2</sup> Moscow Pedagogical State University, Moscow, Russia

¶ e-mail: katikin@mail.ru

Received March 21, 2023

Revised April 14, 2023

Accepted April 17, 2023.

Phantoms are often used to imitate biological tissues in laboratory conditions. Phantoms are usually made on the basis of natural and synthetic materials, as well as hydrogels and various bioactive compositions. Today to visualize biological tissues and study the processes occurring to them in *in vitro* and *in vivo* researches in real time, upconversion nanophosphors (UCNPs) are actively used. They have a whole set of unique photoluminescent properties and are promising components of modern tools for non-invasive optical diagnostics of the human and animals body. We have carried out the synthesis and complex characterization of  $\beta$ -NaYF<sub>4</sub>:Yb<sup>3+</sup>:Er<sup>3+</sup>/NaYF<sub>4</sub> nanoparticles, which effectively convert radiation from the near-IR range into the visible region of the spectrum. The process has been developed to encapsulate them into the structure of aliphatic polyesters and to form bioresorbable polylactoglycolide scaffolds by anti-solvent 3D printing. We formed two types of tissue phantoms based on agarose, ultra-pasteurized cow's milk and melanin. Characterization and analysis of their optical properties were carried out. We studied the transformations of the photoluminescence spectrum of the synthesized UCNPs during the passage of their radiation through these phantoms, and performed the visualization of the photoluminescent polyester matrices placed in them.

**Keywords:** upconversion nanophosphors, photoluminescence, luminescence imaging, biological tissue phantoms, agarose, melanin, aliphatic polyesters.

DOI: 10.61011/EOS.2023.06.56661.124-23

### 1. Introduction

Upconversion nanophosphors (UCNPs) doped with lanthanide ions are highly efficient photoluminescent components of various materials and systems that are extensively used now for non-invasive optical diagnostics of hybrid tissue engineering constructions and biological tissues [1]. They have high structural and chemical stability, bioinertness, narrow bands and large shifts of photoluminescence bands relative to the exciting light wavelength [2], as well as feature stability of their optical characteristics, which distinguish them favorably from other luminophores such as quantum dots or fluorescent proteins [1]. Photoluminescent properties of UCNPs can be actively controlled by doping them with various lanthanide ions. In this way, the properties can be optimized for specific applications. For example, nanoparticles doped with Yb<sup>3+</sup> and Er<sup>3+</sup> ions have the most intense photoluminescence lines at two wavelengths: 544 and 658 nm [3]. This allows monitoring not only their intensity but also the ratio between them, which can be used to visualize and diagnose biological tissue at different depths, taking into account the corresponding dependence of its absorption coefficient and radiation scattering coefficient on the wavelength [4–6].

Biological tissue has a very complex hierarchical structure characterized by many different parameters. Moreover, even for one type of tissue, these parameters can vary within fairly wide limits. So, for example, the optical transmittance of the skin depends on the amount of melanin contained in it [7]. Therefore, phantoms made from various materials of natural or synthetic origin, various hydrogels, and bioactive compositions are often used to simulate biological tissues in laboratory conditions. Usually, in the manufacture of such phantoms, they try to simulate any one property of a particular biological tissue. Phantoms are known that individually simulate dielectric [8,9], acoustic [10], thermophysical [11] or optical [12,13] properties. At the same time, there are also hybrid phantoms (for example, optoacoustic [14,15]) that meet several requirements at once.

The most common phantoms are various structures based on tissues of animal origin [16]. Their parameters are the most similar to those of living biological tissue. However, they are not durable, and it is not always possible to make a phantom of suitable geometric parameters (thickness, size) from them. Synthetic materials for the manufacture of phantoms are divided into solid, semi-solid and liquid [17]. Solid structures are the most stable and can best fit the required geometric parameters. The most common materials for making hard phantoms are polyurethane [18],

silicone [19,20] and wax [21]. Semi-solid materials (or hydrogels) are less stable than solid materials, however, it is much easier to change their composition, if necessary. Most often, phantoms based on agarose [22] and gelatin [23] are used for optical studies. Liquid phantoms are the easiest to manufacture and convenient to change their composition, but at the same time the least stable and durable [24]. To provide phantoms with certain optical properties, various scattering (titanium oxide [25], Liposyn [26], Intralipid [27], milk [28] ) and absorbing (melanin [29], graphite [21] and ink [30]) model media are used.

Objectives of this study are: 1) comprehensive study of the optical properties of biological tissue phantoms based on agarose, ultra-pasteurized cow's milk and melanin that scatter and absorb near-IR and visible radiation, 2) analysis of changes in the spectrum of photoluminescence passing through  $\beta$ -NaYF<sub>4</sub>:Yb<sup>3+</sup>:Er<sup>3+</sup>/NaYF<sub>4</sub> nanoparticles, 3) visualization of photoluminescent polylactoglycolide matrices placed in these phantoms.

## 2. Materials and methods

### 2.1. Synthesis of upconversion nanoparticles

$\beta$ -NaYF<sub>4</sub>:Yb<sup>3+</sup>:Er<sup>3+</sup> (20% Yb, 2% Er) nanoparticles with a NaYF<sub>4</sub> shell were synthesized by thermolysis of precursors in high-boiling (290–310°C) solvents (oleic acid and octadecene) described by the authors earlier [3]. Briefly, a mixture of Y<sub>2</sub>O<sub>3</sub>, Yb<sub>2</sub>O<sub>3</sub>, Er<sub>2</sub>O<sub>3</sub> oxides (Sigma Aldrich, USA) were boiled in the CF<sub>3</sub>COOH:H<sub>2</sub>O=3:1 system until dissolved. To the resulted (CF<sub>3</sub>COO)<sub>3</sub>Y, (CF<sub>3</sub>COO)<sub>3</sub>Yb, (CF<sub>3</sub>COO)<sub>3</sub>Er trifluoroacetates 2 eq (CF<sub>3</sub>COO)Na, 15 ml of 1-octadecene and 15 ml of oleic acid were added. For the decomposition of trifluoroacetates and *in situ* formation of  $\beta$ -NaYF<sub>4</sub>:Yb<sup>3+</sup>:Er<sup>3+</sup> nanocrystals, the flask was placed in Rose's alloy heated to 360°C. After 30 min, the flask was removed from the Rose's alloy, and 15 ml of 1-octadecene was added for rapid cooling. The particles were washed with isopropanol (chemically pure, Ekos-1, Russia) and centrifuged at 6000 rps for 30 min. The reaction was monitored by change in the light transmission of the reaction mixture and in the photoluminescence of the reaction product. The synthesized nanoparticles were covered with a crystalline inert shell of NaYF<sub>4</sub> composition. The inert shell was formed following the procedure described above.

### 2.2. Fabrication of matrices

Poly(lactoglycolide) (PLG) of Purasorb 7507 brand (Corbion Purac, the Netherlands) was used as an initial material for the formation of matrices. The PLG composition for antisolvent formation of the matrix was prepared by dissolving the polymer in tetraglycol (Sigma Aldrich, USA) in a ratio of 10 mas.% [31]. Also, UCNPs were mixed into the composition in a ratio of 1 mas.% of the polymer mass in an ultrasonic bath for 30 min. The finished composition was placed into a silicone mold with a diameter of 5 mm

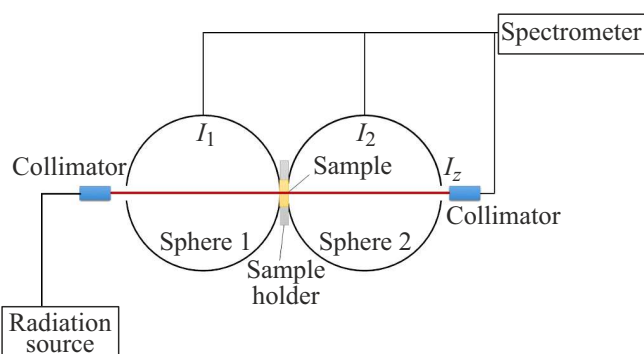


**Figure 1.** Schematic diagram of the setup for determining optical characteristics of phantoms.

and a thickness of 2 mm, fixed at the bottom of the Petri dish, after which the Petri dish was filled with water and left for 24 h until complete curing.

### 2.3. Fabrication of phantoms

Biological tissue phantoms were made on the basis of agarose (Serva, USA). 150 mg of agarose powder was poured into 4 ml of distilled water, heated to 95°C and stirred with a magnetic stirrer until complete dissolution. 3.5% ultra-pasteurized milk (Belgorodsky Molochny Kombinat JSC, Russia) and melanin (Russkie Kornii, Russia) were used as optical model media. To prepare milk-based scattering phantoms, part of distilled water (5 and 10%) was replaced by milk. To prepare absorbing phantoms, melanin was added to the solution with agarose at concentrations of 0.5 and 1 mg/ml. Then the solution with agarose was poured into a Petri dish with a diameter of 6 cm. After complete cooling under normal conditions, Petri dishes with the produced phantoms with a thickness of 1 mm were stored in a refrigerator at a temperature of 4°C. To produce a phantom with a thickness of 2 mm, amounts of all materials were doubled.

### 2.4. Analysis of optical properties

The photoluminescence spectra of the samples excited by a CW radiation of a semiconductor laser with a wavelength of 976 nm were recorded using a Fluorolog-3 spectrofluorimeter (Horiba Jobin Yvon, France). The transmission coefficient of phantoms was measured by a Cary 50 spectrophotometer (Varian, USA). To record the photoluminescence spectrum through a phantom, it was placed immediately on top of the sample. To assess the change in the photoluminescence spectrum of UCNPs as a result of the interaction with the phantom, 40  $\mu$ l of a colloidal solution of nanoparticles in hexane (with a concentration of 17.5 mg/ml) was applied to paper (1  $\times$  1 cm, Fax Standard 210 mm, Russia).

The optical characteristics of the phantom were measured using a setup (Fig. 1) based on two integrating spheres

(with a diameter of 75 mm) [32], coated from inside with a standard diffusely scattering material. The phantom sample was placed between the spheres. White light radiation from a HL-2000 halogen source (Ocean Optics, USA) was introduced into sphere 1. The emission spectra in the spheres were recorded using a USB4000 spectrometer (Ocean Optics, USA) with a wavelength range of 200–1100 nm.

To calculate the coefficients of diffuse scattering  $R_d$ , diffuse transmission  $T_d$  and collimated transmission  $T_c$ , the following relations were used [28,32]:

$$R_d = \frac{I_1}{I_{01}}, T_d = \frac{I_2}{I_{01}}, T_c = \frac{I_z}{I_{0z}},$$

$$-\ln(T_c)/d = (\mu_a + \mu_s),$$

where  $I_{01}$  is radiation intensity in sphere 1 with a plug covered with a standard diffusely scattering material installed instead of the sample,  $I_1$  is radiation intensity in sphere 1 in the presence of sample,  $I_2$  is intensity in sphere 2 in the presence of the sample,  $I_{0z}$  is radiation intensity at the outlet from sphere 2 without the sample,  $I_z$  is radiation intensity at the outlet from sphere 2 with the sample,  $\mu_a$  is absorption coefficient,  $\mu_s$  is scattering coefficient,  $d$  is phantom thickness.

Based on the obtained experimental data (diffuse scattering coefficients  $R_d$ , diffuse transmission  $T_d$  and collimated transmission  $T_c$ ), the optical characteristics of phantoms were calculated using the Monte Carlo method described in [32]. Briefly, the MatLab software package allows solving the direct problem of determining the  $R_d$ ,  $T_d$  and  $T_c$  coefficients from pre-defined parameters: the  $g$  anisotropy factor and  $\mu_s$  and  $\mu_a$  coefficients. By varying these parameters, it is possible to solve the problem and find the values of the  $R'_d$  and  $T'_d$  coefficients, which are most consistent with the experimental ones. To do this, it is necessary to determine the minimum of the following expression:

$$\varepsilon = \frac{(R'_d - R_d)^2}{R_d^2} + \frac{(T'_d - T_d)^2}{T_d^2}.$$

To visualize the UCNPs embedded in matrices, the imaging system described in [33] equipped with a Raylase scanner head (Germany) was used, which deflects the infrared laser beam along the  $x$  and  $y$  axes. The signal is recorded using an EMCCD camera (Raptor Photonics Incorporated, USA) with a high sensitivity in the range of 400–850 nm and a laser galvanometric scanner controlled from a PC (Ateko Technocenter, Russia) for accurate targeting of the laser beam to the sample. A LDD-10 semiconductor laser (Poluprovodnikovye pribory JSC, Russia) with a fiber output was used as a light source at a wavelength of 976 nm. The intensity of laser radiation was 200 mW/cm<sup>2</sup>. The camera was focused using an optical lens with  $F = 0.95$ , and a system of interference filters (Semrock, USA) was used to cut off the exciting radiation (976 nm).

The intensity of photoluminescence of nanoparticles impregnated into the matrix was quantitatively evaluated using the ImageJ software [34].

Plotting was performed in the OriginPro 9 software (OriginLab, USA), statistical processing of the results was carried out in Microsoft Excel (Microsoft, USA). Under normal distribution, Student's t-test was used to compare two values. Differences were considered statistically significant if the error probability of rejecting the null hypothesis was below 5% ( $p < 0.05$ ).

### 3. Results and discussions

#### 3.1. $\beta$ -NaYF<sub>4</sub>:Yb<sup>3+</sup>:Er<sup>3+</sup> (NaYF<sub>4</sub>) core/shell type UCNPs

Upconversion nanoparticles of the core/shell type with an average diameter of 21±6 nm were used in the experiments. The photoluminescence spectra and the ratio of the intensities of the „red“ peak at 658 nm to the intensity of the „green“ peak at a wavelength of 544 nm for these UCNPs are shown in Fig. 2. The R/G intensity ratio of the initial nanoparticles increases with increasing power density of the exciting radiation and does not exceed 0.6 at a power density of 300 W/cm<sup>2</sup>, which is indicative of a high intensity of the „green“ peak, provided that the nanoparticles do not interact with anything. That is why these particles were chosen, because the contribution of the red peak will only increase with further manipulations.

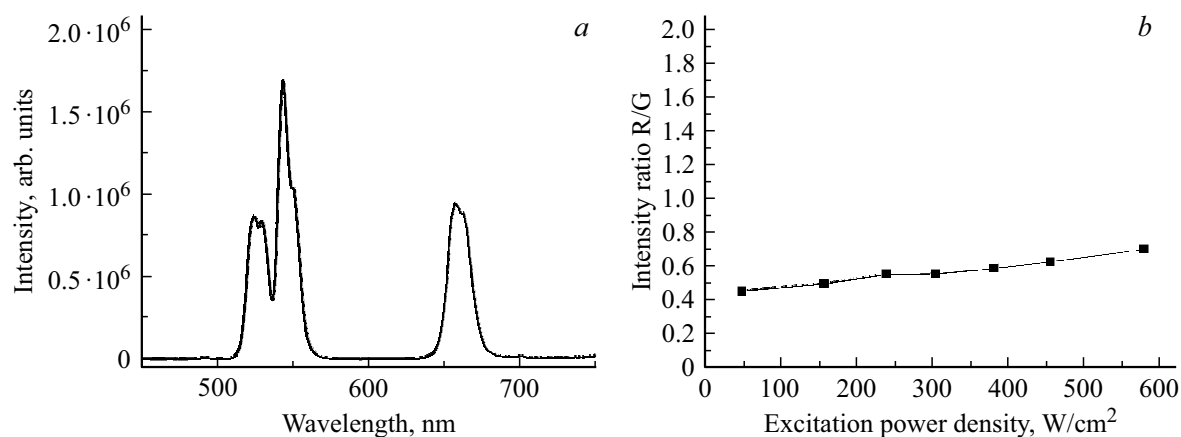
#### 3.2. UCNPs-impregnated matrices

The photoluminescence spectrum of UCNPs embedded in the PLG-matrix (Fig. 3) is different because the nanoparticles surround polymer molecules. The intensity ratio now does not exceed 1.4 at a power density of the exciting radiation of 300 W/cm<sup>2</sup>. Then all photoluminescence spectra and intensity ratios obtained using a phantom will be compared with the data of UCNPs embedded in the PLG-matrix.

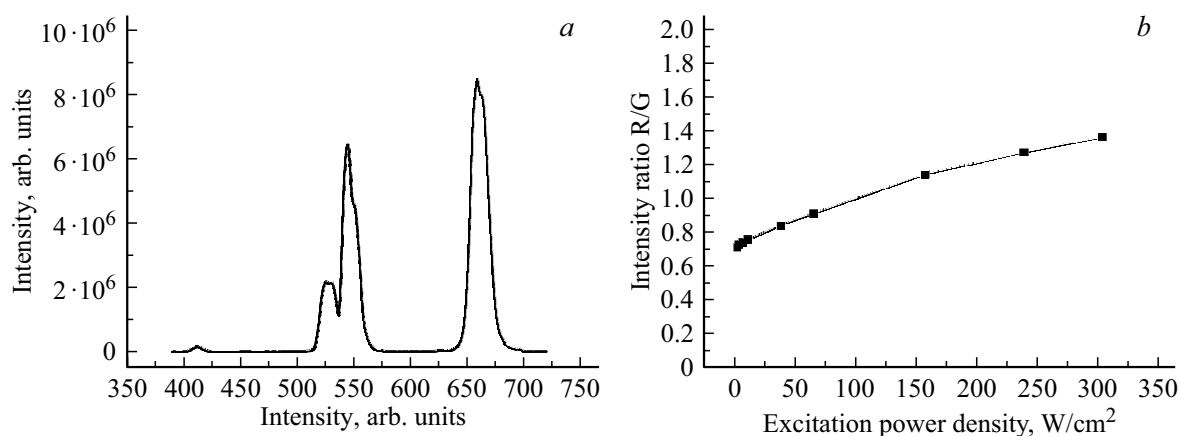
#### 3.3. Optical properties of phantoms

Fig. 4 shows the transmission coefficients  $T$  of phantoms depending on the wavelength. The transmission coefficient  $T$  decreases both with an increase in the concentration of the model substance (milk and melanin) and with an increase in the thickness of the phantom. In the visible range, this is not so pronounced for milk-based phantoms, in contrast to melanin-based phantoms. Based on the data for the transmission coefficient, it can be seen that the minimum intensity of photoluminescence is recorded using an agarose-based phantom with the addition of 10% milk with a thickness of 2 mm

Using a setup with two integrating spheres, the dependences of the diffuse scattering coefficients  $R_d$  for all phantoms were obtained (Tables 1 and 2). It can be seen



**Figure 2.** Photoluminescence spectrum of UCNPs with the  $\beta$ -NaYF<sub>4</sub>:Yb<sup>3+</sup>:Er<sup>3+</sup> core/shell structure (a); dependence of the ratio between the „red“ intensity peak at 658 nm and the „green“ intensity peak at a wavelength of 544 nm on the laser radiation power density for core/shell type UCNPs (b).



**Figure 3.** Photoluminescence spectrum of  $\beta$ -NaYF<sub>4</sub>:Yb<sup>3+</sup>:Er<sup>3+</sup> UCNPs embedded in PLG-matrices (a). Dependence of the ratio between the „red“ intensity peak at 658 nm and the „green“ intensity peak at a wavelength of 544 nm on the laser radiation power density for core/shell type UCNPs (b).

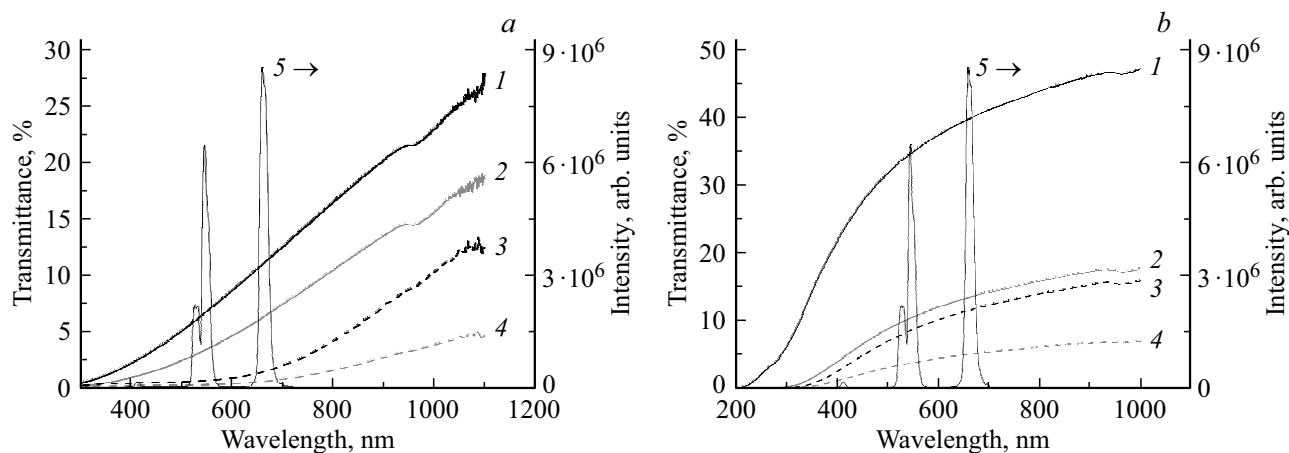


**Figure 4.** Transmission coefficient of agarose-based phantoms with different milk content (a): 1 — 5% with a thickness of 1 mm, 2 — 5% with a thickness of 2 mm, 3 — 10% with a thickness of 1 mm, 4 — 10% with a thickness of 2 mm and melanin (b): 1 — 0.5 mg/ml with a thickness of 1 mm, 2 — 0.5 mg/ml with a thickness of 2 mm, 3 — 1 mg/ml with a thickness of 1 mm, 4 — 1 mg/ml with a thickness of 2 mm. Curves 5 (on both plots) — photoluminescence spectrum of  $\beta$ -NaYF<sub>4</sub>:Yb<sup>3+</sup>:Er<sup>3+</sup> UCNPs embedded in PLG-matrices.

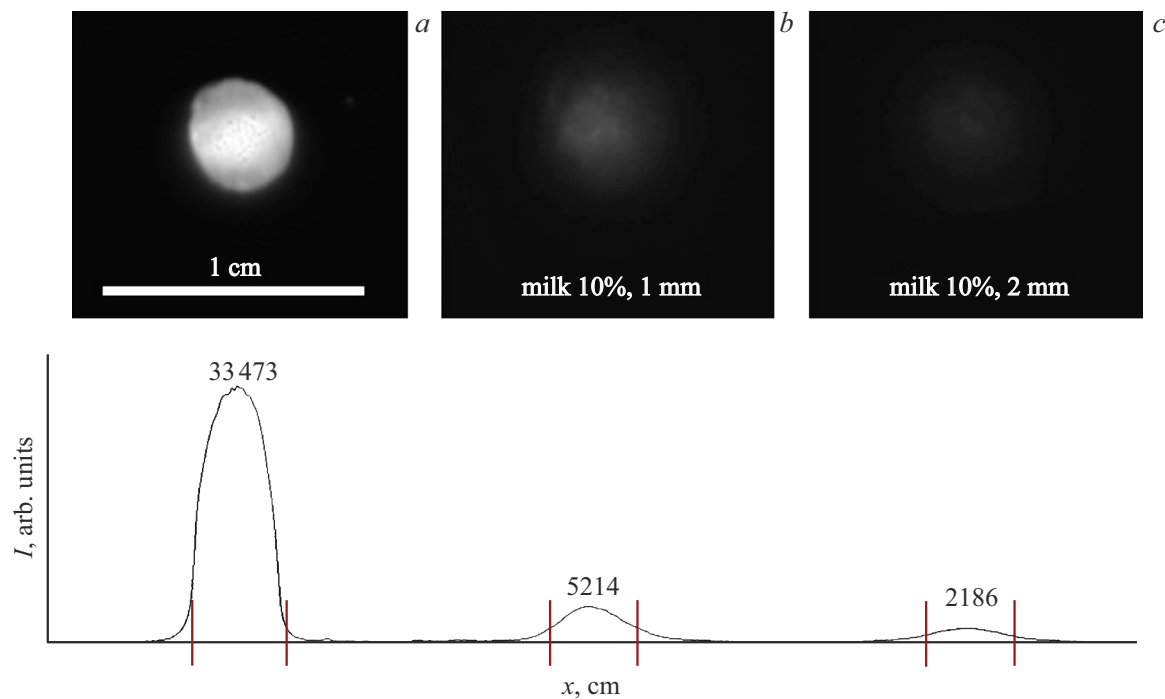


**Figure 5.** Photo of the original matrix (a) and photos through phantoms with the addition of 10% milk 1 mm (b) and 2 mm (c) and the corresponding intensity analysis. Red lines show boundaries of the sample.

from the tables that at a wavelength of 544 nm this coefficient has a greater value than at wavelengths of 658 and 980 nm, and only monotonically increases with increasing concentration of the model substance. Based on the obtained experimental data (diffuse scattering coefficients  $R_d$ , diffuse transmission  $T_d$  and collimated transmission  $T_c$ ), the optical characteristics of phantoms were calculated using the Monte Carlo method described in [32] for three wavelengths of 544, 658 and 976. Anisotropy factor  $g$ , absorption coefficient  $\mu_a$  and scattering coefficient  $\mu_s$  for all phantoms are calculated. It can be seen from Table 1 that the  $g$  coefficient grows with increase in both the wavelength and the quantity of scatter. The scattering coefficient increases with increase in the amount of milk at all wavelengths.

The optical properties of biological tissues vary greatly depending on their type and composition. Even within the same type of tissue (for example, skin), different values of absorption coefficients  $\mu_a$  and scattering coefficients  $\mu_s$  can be found in the literature for the same wavelength. Thus, in [35], for the skin of different patients,  $\mu_a$  at a wavelength of 500 nm varies in the range from 3.8 to 15.3. Thus, by choosing the optimal concentration of the scattering and absorbing components of the model media, optical properties of a particular biological tissue can be modeled.

### 3.4. Visualization of UCNP-impregnated matrices

Changes in the photoluminescence spectra of UCNPs embedded in the matrix can occur both due to absorption and scattering of radiation by the phantom. Due to the fact

that the exciting radiation passed through the phantom, at the same input radiation power, the power density of the exciting radiation changed and was calculated taking into account the transmission coefficient of the phantom.

An example of visualization of matrices through the phantoms in the visible range is shown in Fig. 5 and 6. It can be seen that as the thickness of the phantom increases, the integrated intensity at wavelengths of 544 and 658 nm decreases. This is confirmed both by the analysis of the obtained images and by the calculated optical characteristics from Table 1. When calculating the intensity quantitatively, it can be seen that the lowest photoluminescence intensity (in arbitrary units) is observed when the radiation passes through a phantom with 10% milk with a thickness of 2 mm, which is in good agreement with Fig. 4. Moreover, due to the scattering of radiation, the boundaries of the sample become less clear when it is visualized through phantoms. For phantoms with the addition of milk, the value of the integrated photoluminescence intensity is much lower (by 60–70%) than that for the phantoms with the addition of melanin.

## 4. Conclusion

As a result of the experiments, the optical characteristics of two types of phantoms of biological tissues made on the basis of scattering and absorbing model media were studied depending on the thickness of the phantom and the concentration of its constituent substances. Changes

**Table 1.** Experimental values of  $R_d$  and  $T_d$ , as well as calculated optical characteristics of phantoms based on agarose with the addition of melanin. (Statistical processing of the factor  $g$ , as well as the coefficients  $\mu_s$  and  $\mu_a$  is presented with an error of  $\pm 0.05$ ,  $3 \text{ cm}^{-1}$  and  $0.05 \text{ cm}^{-1}$ , respectively.)

Phantom type	Wavelength, nm	$R_d$	$T_d$	$\mu_s, \text{cm}^{-1}$	$\mu_a, \text{cm}^{-1}$	$g$
Milk 5%, 1 mm	544	0.65	0.31	42	0.20	0.15
	658	0.40	0.51	36	0.45	0.60
	976	0.33	0.59	30	0.50	0.65
Milk 5%, 2 mm	544	0.58	0.34	74	0.35	0.60
	658	0.31	0.61	86	0.45	0.90
	976	0.28	0.59	82	0.75	0.90
Milk 10%, 1 mm	544	0.49	0.47	59	0.15	0.70
	658	0.45	0.51	57	0.25	0.70
	976	0.39	0.53	43	0.60	0.70
Milk 10%, 2 mm	544	0.50	0.41	106	0.20	0.80
	658	0.46	0.51	116	0.25	0.85
	976	0.38	0.48	110	0.50	0.90

**Table 2.** Experimental values of  $R_d$  and  $T_d$ , as well as calculated optical characteristics of phantoms based on agarose with the addition of melanin. (Statistical processing of the factor  $g$ , as well as the coefficients  $\mu_s$  and  $\mu_a$  is presented with an error of  $\pm 0.1$ ,  $2 \text{ cm}^{-1}$  and  $0.05 \text{ cm}^{-1}$ , respectively.)

Phantom type	Wavelength, nm	$R_d$	$T_d$	$\mu_s, \text{cm}^{-1}$	$\mu_a, \text{cm}^{-1}$	$g$
Melanine 0.5 mg/ml, 1 mm	544	0.65	0.25	17	1.5	0.1
	658	0.34	0.45	15	1.5	0.1
	976	0.33	0.50	13	1.5	0.1
Melanine 0.5 mg/ml, 2 mm	544	0.67	0.18	44	4	0.3
	658	0.31	0.20	40	4	0.5
	976	0.34	0.23	34	3	0.3
Melanine 1 mg/ml, 1 mm	544	0.59	0.14	27	7	0.1
	658	0.26	0.15	25	6	0.1
	976	0.25	0.20	20	5	0.1
Melanine 1 mg/ml, 2 mm	544	0.56	0.06	55	9	0.5
	658	0.24	0.08	53	8	0.5
	976	0.22	0.09	46	8	0.5

in the photoluminescence spectra of  $\beta\text{-NaYF}_4\text{:Yb}^{3+}\text{:Er}^{3+}$  UCNPs with the core/shell structure are analyzed. The intensity ratios between the „red“ peak at 658 nm of UCNP photoluminescence and the intensity of the „green“ peak at a wavelength of 544 nm are calculated depending on the type of phantom, its thickness, and the concentration of model substances. It is shown that with an increase in both the thickness of the phantom with the addition

of melanin and the concentration of this substance, the intensity ratio between „red“ photoluminescence peak (at a wavelength of 658 nm) of both the initial UCNPs and the UCNPs contained in PLG-matrices (placed in these phantoms) and the intensity of the „green“ peak (at a wavelength of 544 nm) increase at the same power density of the absorbing radiation.

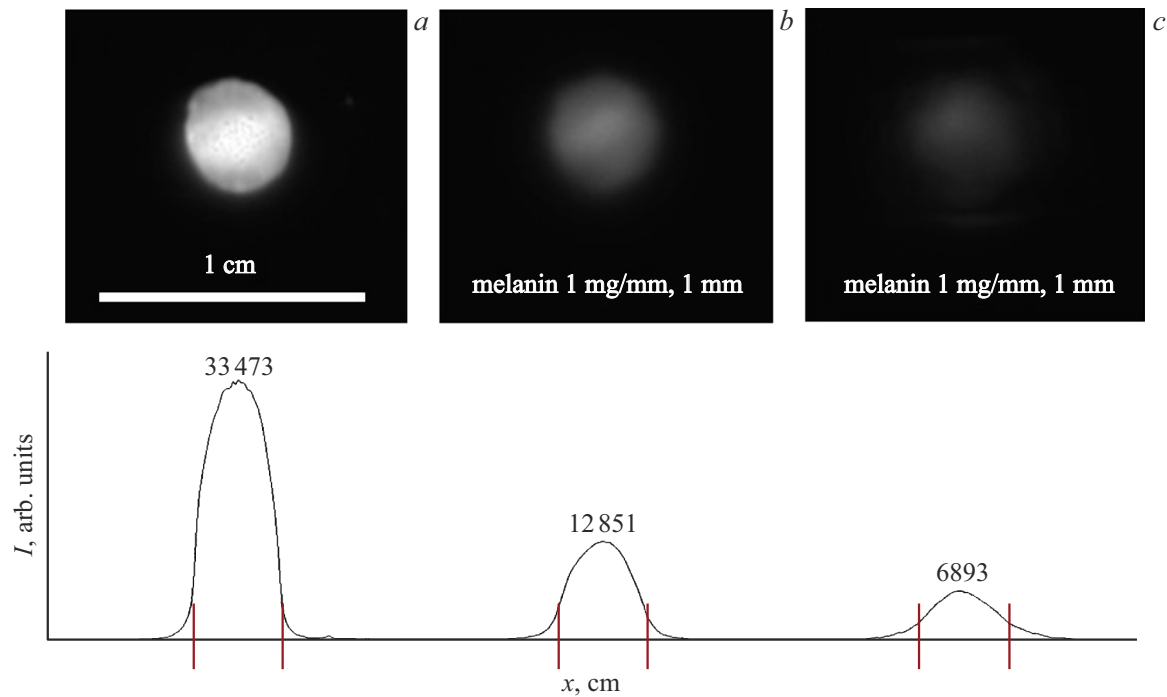


**Figure 6.** Photo of the original matrix (a) and photos through phantoms with the addition of 1 mg/ml of melanin 1 mm (b) and 2 mm (c) and the corresponding intensity analysis. Red lines show boundaries of the sample.

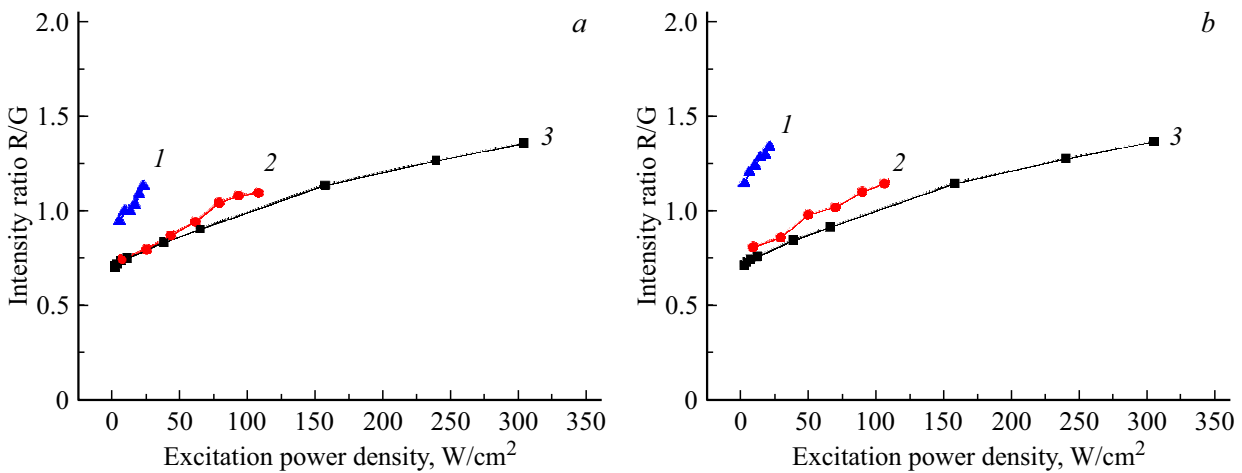


**Figure 7.** Dependence of the intensity ratio between the „red“ peak at 658 nm and the „green„ peak at a wavelength of 544 nm for UNPs embedded in the PLG-matrix (curve 3 on the graphs a and b) on the power density of laser radiation through agarose-based phantoms with milk: (a) 1 — 5% with a thickness of 2 mm, 2 — 5% with a thickness of 1 mm; (b) 1 — 10% with a thickness of 2 mm, 2 — 10% with a thickness of 1 mm.

At the same time, not only the integral intensity changes but also the ratio between the intensity of the „red“ peak at 658 nm and the intensity of the „green“ peak at a wavelength of 544 nm (R/G) (Fig. 7). For UCNP-embedded in the PLG-matrix, with an increase in the content of the model scattering substance, the intensity of the red peak increases. For phantoms with a thickness of 1 mm, the difference in milk concentration is not as noticeable as for phantoms with a thickness of 2 mm. As the concentration

increases from 5 to 10%, the R/G ratio increases from 1.17 to 1.3. This can be explained by the Mie scattering effect: the longer is the wavelength, the lower is the intensity of the scattered light [36].

Also, the „red“/„green“ ratios were calculated for nanoparticles embedded in the matrix, depending on the phantom with melanin located between the matrix and the detector (Fig. 8). As the thickness of the phantom increases, the intensity of the „red“ peak at 658 nm

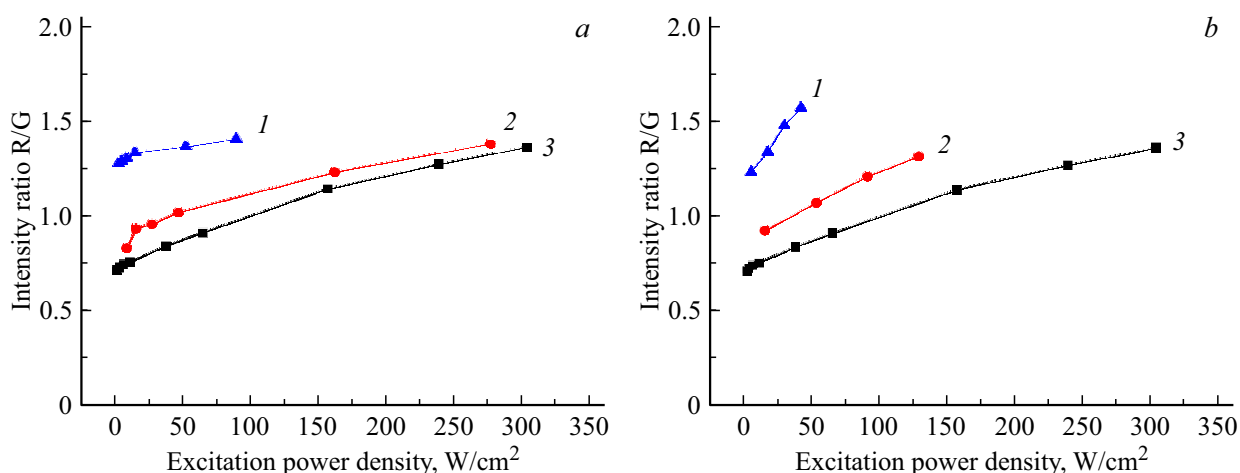


**Figure 8.** Dependence of the intensity ratio between the „red“ peak at 658 nm and the “green,” peak at a wavelength of 544 nm for UNPs embedded in the PLG-matrix (curve 3 on the graphs *a* and *b*) on the power density of laser radiation through agarose-based phantoms with melanin: (*a*) 1 — 0.5% with a thickness of 2 mm, 2 — 0.5% with a thickness of 1 mm; (*b*) 1 — 1% with a thickness of 2 mm, 2 — 1% with a thickness of 1 mm.

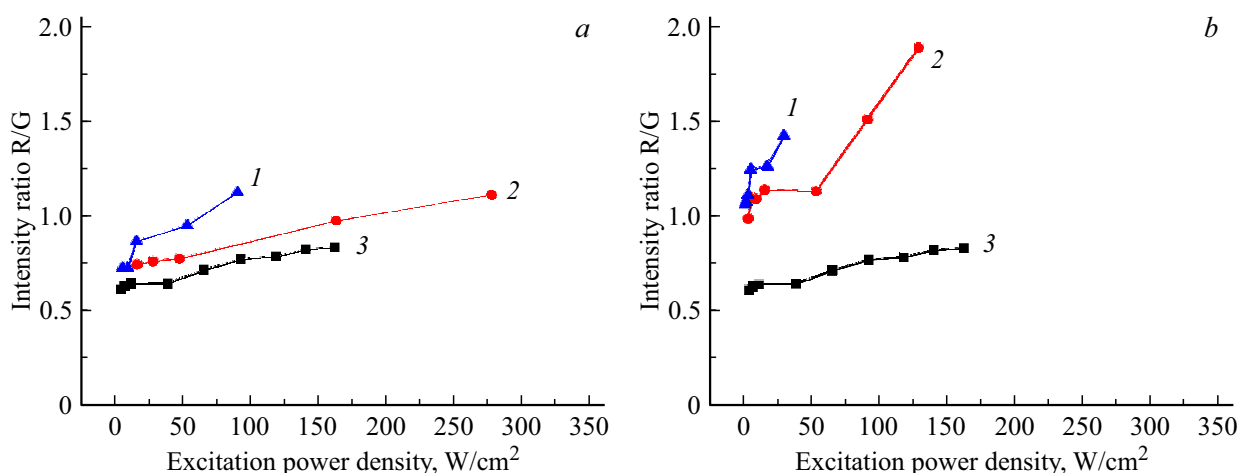


**Figure 9.** Dependence of the intensity ratio between the „red“ peak at 658 nm and the “green,” peak at a wavelength of 544 nm for UNPs applied on paper (curve 3 on the graphs *a* and *b*) on the power density of laser radiation through agarose-based phantoms with melanin: (*a*) 1 — 0.5% with a thickness of 2 mm, 2 — 0.5% with a thickness of 1 mm; (*b*) 1 — 1% with a thickness of 2 mm, 2 — 1% with a thickness of 1 mm.

increases, in the same way as it does with the increase in the melanin concentration in general. This can be explained by several reasons. As the phantom thickness increases, the transmission coefficient at a wavelength of 658 nm decreases by a factor of 3, and at a wavelength of 544 nm it decreases by a factor of 3.4. With an increase in the concentration of melanin, a similar behavior is observed.

The change in the photoluminescence spectrum of UCNPs applied on paper upon interaction with a phantom was studied (Fig. 9). In this experiment, UCNPs are not located inside the matrix; therefore, they are not covered by a protective polymer layer and can interact directly with the phantom substance.

Due to the interaction of UCNPs with water, the photoluminescence spectrum of the particles changes: the

intensity of the „red“ peak increases due to nonradiative transitions [37]. Therefore, when interacting with a phantom, it is expected that the intensity of the „red“ peak will also increase: for the initial nanoparticles at a laser radiation power density of 150 W/cm<sup>2</sup>, this coefficient is equal to 0.5, and for UNPs applied on paper and interacting with the phantom, it is more than 0.8. Thus, when calculating the intensity ratio, it is necessary to take into account not only the optical properties of the phantom but also the influence of the environment of the nanoparticles themselves.

#### Funding

The work was carried out within the framework of the State Assignment of the „Crystallography and Photonics“

Federal Research Center of RAS (as related to the synthesis of upconversion nanophosphors and production of phantoms of biological tissues) and the RFBR grant (project № 20-32-90218) as related to the characterization and visualization of polyester matrices.

### Conflict of interest

The authors declare that they have no conflict of interest.

### References

- [1] L. Cheng, K. Yang, S. Zhang, M. Shao, S. Lee, Z. Liu. *Nano Res.*, **3** (10), 722 (2010). DOI: 10.1007/s12274-010-0036-2
- [2] J. Zhou, Z. Liu, F. Li. *Chem. Soc. Rev.*, **41** (3), 1323 (2012). DOI: 10.1039/C1CS15187H
- [3] E.M. Trifanova, M.E. Nikolaeva, V.K. Popov, *Perspektivnye materialy*, **12**, 40 (2021) (in Russian). DOI: 10.30791/1028-978X-2021-12-40-50
- [4] E. Hemmer, N. Venkatachalam, H. Hyodo, A. Hattori, Y. Ebina, H. Kishimoto, K. Soga. *Nanoscale*, **5** (23), 11339 (2013). DOI: 10.1039/c3nr02286b
- [5] L. Bachmann, D.M. Zezell, A. da C. Ribeiro, L. Gomes, A.S. Ito. *Appl. Spectrosc. Rev.*, **41** (6), 575 (2006). DOI: 10.1080/05704920600929498
- [6] *Laser-induced interstitial thermotherapy*, ed. by A. Roggan, G. Muller (SPIE Press, Bellingham, WA, 1995), p. 10–44.
- [7] M. Lualdi, A. Colombo, A. Mari, S. Tomatis, R. Marchesini. *J. Laser Appl.*, **14** (2), 122 (2002). DOI: 10.2351/1.1475339
- [8] C. Ianniello, J.A. de Zwart, Q. Duan, C.M. Deniz, L. Alon, J.S. Lee, R. Lattanzi, R. Brown. *Magn. Reson. Med.*, **80** (1), 413 (2018). DOI: 10.1002/mrm.27005
- [9] B.L. Oliveira, D. O’Loughlin, M. O’Halloran, E. Porter, M. Glavin, E. Jones. *Biomed. Phys. Eng. Express*, **4** (2), (2018). DOI: 10.1088/2057-1976/aaaaff
- [10] K. Zell, J.I. Sperl, M.W. Vogel, R. Niessner, C. Haisch. *Phys. Med. Biol.*, **52** (20), 475 (2007). DOI: 10.1088/0031-9155/52/20/N02
- [11] A.V. Kondyurin, A.P. Sviridov. *Quantum Electron.*, **38** (7), 641 (2008).
- [12] B.W. Pogue, M.S. Patterson. *J. Biomed. Opt.*, **11** (4), 041102 (2006). DOI: 10.1117/1.2335429
- [13] *Handbook of Optical Biomedical Diagnostics*, ed. by V.V. Tuchin (SPIE Press, Bellingham, WA, 2002), ch. 5, p. 311–354.
- [14] E. Amidi, G. Yang, K.M.S. Uddin, R. Wahidi, Q. Zhu. In: *Photons Plus Ultrasound: Imaging and Sensing 2019*, ed. by A.A. Oraevsky, L.V. Wang (SPIE Press, San Francisco, CA, 2019), p. 157. DOI: 10.1117/12.2507938
- [15] E. Maneas, W. Xia, O. Ogunlade, M. Fonseca, D.I. Nikitichev, A.L. David, S.J. West, S. Ourselin, J.C. Hebden, T. Vercauteren, A.E. Desjardins. *Biomed. Opt. Express*, **9** (3), 1151 (2018). DOI: 10.1364/boe.9.001151
- [16] S. Mosca, P. Lanka, N. Stone, S. Konugolu Venkata Sekar, P. Matousek, G. Valentini, A. Pifferi. *Biomed. Opt. Express*, **11** (3), 1697 (2020). DOI: 10.1364/boe.386349
- [17] M.Z. Vardaki, N. Kourkoumelis. *Biomed. Eng. Comput. Biol.*, **11**, 117959722094810 (2020). DOI: 10.1177/1179597220948100
- [18] T. Moffitt, Y.-C. Chen, S.A. Prahl. *J. Biomed. Opt.*, **11** (4), 041103 (2006). DOI: 10.1117/1.2240972
- [19] S.K.V. Sekar, A. Pacheco, P. Martella, H. Li, P. Lanka, A. Pifferi, S. Andersson-Engels. *Biomed. Opt. Express*, **10** (4), 2090 (2019). DOI: 10.1364/BOE.10.002090
- [20] S.K.V. Sekar, A. Pacheco, P. Martella, H. Li, P. Lanka, A. Pifferi, S. Andersson-Engels. In: *European Conference on Biomedical Optics*, ed. by H. Dehghani, H. Wabnitz (Optica Publishing Group, 2019), p. 11074-46. DOI: 10.1117/12.2526867
- [21] E. Dong, Z. Zhao, M. Wang, Y. Xie, S. Li, P. Shao, L. Cheng, R.X. Xu. *J. Biomed. Opt.*, **20** (12), 121311 (2015). DOI: 10.1117/1.JBO.20.12.121311
- [22] A. Mustari, I. Nishidate, M.A. Wares, T. Maeda, S. Kawachi, S. Sato, M. Sato, Y. Aizu. *J. Vis. Exp.*, **2018** (138), (2018). DOI: 10.3791/57578
- [23] P. Lai, X. Xu, L.V. Wang. *J. Biomed. Opt.*, **19** (3), 035002 (2014). DOI: 10.1117/1.JBO.19.3.035002
- [24] D.A. Loginova, E.A. Sergeeva, A.D. Krainov, P.D. Agrba, M.Y. Kirillin. *Quantum Electron.*, **46** (6), 528 (2016). DOI: 10.1070/QEL16133
- [25] G.M. Spirou, A.A. Oraevsky, I.A. Vitkin, W.M. Whelan. *Phys. Med. Biol.*, **50** (14), 141 (2005). DOI: 10.1088/0031-9155/50/14/N01
- [26] J. Sun, K. Fu, M.-Q. Zhu, L. Bickford, E. Post, R. Drezek. *Curr. Nanosci.*, **5** (2), 160 (2009). DOI: 10.2174/157341309788185433
- [27] J.R. Cook, R.R. Bouchard, S.Y. Emelianov. *Biomed. Opt. Express*, **2** (11), 3193 (2011). DOI: 10.1364/boe.2.003193
- [28] C. Fajardo, E. Solarte. *J. Phys. Conf. Ser.*, **1547** (1), 012026 (2020). DOI: 10.1088/1742-6596/1547/1/012026
- [29] G. Zonios, J. Bykowski, N. Kollias. *J. Invest. Dermatol.*, **117** (6), 1452 (2001).
- [30] P. Di Ninni, F. Martelli, G. Zaccanti. *Opt. Express*, **18** (26), 26854 (2010). DOI: 10.1364/OE.18.026854
- [31] A.V. Mironov, O.A. Mironova, M.A. Syachina, V.K. Popov. *Polymer (Guildf)*, **182** (July), 121845 (2019). DOI: 10.1016/j.polymer.2019.121845
- [32] A.P. Sviridov, V.S. Zhigarkov, A.G. Shubny, V.I. Yusupov. *Quantum Electronics* **50** (1), 81, (2020). DOI: 10.1070/QEL17236
- [33] A.N. Generalova, I.K. Kochneva, E.V. Khaydukov, V.A. Semchishen, A.E. Guller, A.V. Nechaev, A.B. Shekhter, V.P. Zubov, A.V. Zvyagin, S.M. Deyev. *Nanoscale*, **7** (5), 1709 (2015). DOI: 10.1039/C4NR05908E
- [34] C.A. Schneider, W.S. Rasband, K.W. Eliceiri. *Nat. Methods*, **9** (7), 671 (2012). DOI: 10.1038/nmeth.2089
- [35] V.V. Tuchin. *Optika biologicheskikh tkanei. Metody rasseyaniya sveta v meditsinskoy diagnostike* (FIZMATLIT, Moscow, 2012), p. 275–390 (in Russian).
- [36] G. Mie. *Ann. Phys.*, **331** (8), 597 (1908)
- [37] N. Bogdan, F. Vetrone, G.A. Ozin, J.A. Capobianco. *Nano Lett.*, **11** (2), 835 (2011). DOI: 10.1021/nl1041929

Translated by Y.Alekseev